

Contents lists available at ScienceDirect

Wear

journal homepage: www.elsevier.com/locate/wear





Effect of fictive temperature on tribological properties of Zr₄₄Ti₁₁Cu₁₀Ni₁₀Be₂₅ bulk metallic glasses

Shipra Bajpai ^{a, 1}, Ambreen Nisar ^{a, c, 1}, Rupesh Kumar Sharma ^a, Udo D. Schwarz ^b, Kantesh Balani ^{a, **}, Amit Datye ^{b, *}

- ^a Department of Materials Science and Engineering, Indian Institute of Technology, Kanpur, Kanpur, UP, 208016, India
- ^b Department of Mechanical Engineering and Materials Science, Yale University, New Haven, CT, 06511, USA
- ^c Department of Mechanical and Materials Engineering, Florida International University, Miami, FL, 33174, USA

ARTICLE INFO

Keywords: Bulk metallic glasses Fictive temperature Nano indentation Micro-scratching

ABSTRACT

Zirconium (Zr) based bulk metallic glasses (BMGs) have emerged as a potential material for various engineering applications due to their unique and tunable mechanical properties. Heat treatment of the BMGs plays a vital role in changing the mechanical as well as tribological properties. In the present work, the effect of the fictive temperature (T_f) on the mechanical and tribological behavior of Zr based BMGs with a glass transition temperature (T_g) of 352 °C has been studied by nanoindentation and micro-scratch testing at constant (load 10 N) and progressive (0.5-25 N) loading conditions. The BMGs were heat treated at three different fictive temperatures ranging from $0.91T_g$ (320 °C) to $1.05T_g$ (370 °C). Hardness and effective elastic modulus were observed to be highest (8.3 GPa and 128 GPa, respectively) for the metallic glass with a fictive temperature of $0.91T_{\rm g}$ (320 °C). With an increase in fictive temperature, hardness and effective elastic modulus decrease due to decreased short-range ordering and more free volume (density fluctuations) in the internal structure, which enhances atomic and plastic flow in the material. For constant loading, wear resistance is observed to be similar for as-cast BMG and BMG with $T_{\rm f}=1.05T_{\rm g}$, but increases by 65% and 40% from as-cast to BMGs with $T_{\rm f}$'s of $0.91T_{\rm g}$ and 0.99Tg, respectively. For progressive loading, the wear resistance increases by 10% from as-cast to 0.91Tg, whereas it decreases by 75% and 76% as T_f increases to $0.99T_g$ and $1.05T_g$, respectively. BMGs with $T_f = 0.91T_g$ are observed to be the most wear resistant in both the loading conditions, making it a viable candidate for biomedical applications, machine tools, and engine parts where wear resistance of the component during service is a dominating factor.

1. Introduction

Bulk metallic glasses (BMGs), which were first developed in 1960 [1], show unusual mechanical, physical and chemical properties when compared to the conventional materials [2–4]. Initially ribbons (<100 μ m) and thin films were formed by rapid quenching (10^5 – 10^6 K/s) [5] to avoid the crystallization in the materials. Later on, in the 1970ies and 1980ies, research led to the development of numerous ternary alloys systems that could be cooled at slower cooling rates resulting in the formation of BMGs with thicknesses (as smallest dimension) of larger than 1 mm [6–8]. In daily life, bulk metallic glasses are being used for numerous applications ranging from eyeglass frames, sports equipment,

precision parts, aerospace equipment [2,3,5,9] to biomedical implants [2,9,10]. High glass forming ability, good mechanical properties and better wear resistance of the glassy alloys enables them to be used in the applications involving mechanical parts such as precision gears etc.

In conventional polycrystalline metals and alloys, ordered atomic structure along with the presence of defects like dislocations and grain boundaries, etc. results in plastic deformation in response to external stress. In contrast to polycrystalline materials, BMGs possess only short-range atomic order, which leads to inhomogeneous deformation with a range of deformation mechanisms [12–14] at larger length scales. Nanoindentation study on the Ti-based BMGs suggests that the

^{**} Corresponding author.

^{*} Corresponding author.

E-mail addresses: kbalani@iitk.ac.in (K. Balani), amit.datye@yale.edu (A. Datye).

¹ Equally contributed as first author.

generation of shear bands in metallic glasses is controlled by the atomic scale rearrangement, which again is dependent on the structural state as well as the deformation history of the metallic glass [15]. Bulk metallic glasses are expected to have higher wear resistance owing to their superior mechanical properties; however, there are some studies which report that the tribological behavior of BMGs is inferior to their crystalline [16] as well as annealed (relaxed) alloys [17].

In a recent study, Salehan et al. [18] reported the wear behavior of Zr based bulk metallic glasses that are annealed at different temperatures by sliding against AISI52100 steel. Results indicated that the relaxed samples had shown the lowest wear rate compared to the as-cast and crystallized samples. In the case of the as-cast and relaxed samples, abrasive wear was the dominant wear mechanism whereas it changes to the brittle fracture for partially and fully crystallized samples leading to the higher wear rate. Similar results were also reported by Liu et al. [19] where the wear behavior of Zr_{52.5}Cu_{17.9}Al₁₀Ni_{14.6}Ti₅ metallic glasses with different crystallinity was tested by pin-on disc wear test. It was observed that the wear loss and coefficient of friction (CoF) does not have any direct relationship with hardness or crystallinity however wear mechanism changes with the introduction of crystalline phases. They also reported that the wear behavior of the metallic glasses does not follow the Archard's law, however a good combination of hardness and fracture toughness both can make a bulk metallic glass to be wear resistant. In a similar study by Bhatt et al. [20], e.g., friction and dry sliding behavior of as-cast Cu₆₀Zr₃₀Ti₁₀ glassy alloys have been compared with the same alloy annealed at two different temperatures (450 $^{\circ}$ C and 522 $^{\circ}$ C, respectively) for 1 h. Thereby, the annealing at 450 °C was intended to only relieve residual stresses whereas a crystallized structure has been obtained by annealing at 522 °C. Under these circumstances, the CoF is reported to be in the range of 0.3-0.4, with its lowest value being observed for as-cast BMG and the highest value for the relaxed BMG. The latter also showed the highest hardness and wear resistance, followed by the as-cast BMG and finally the alloy obtained after crystallization. This observation can be rationalized by considering that when crystallized, crack initiation and propagation can occur along the alloy's glide planes that decrease its overall wear resistance. Another study by Parler et al. [21] on the dry sliding behavior of Zr-based BMGs at different loads and velocities shows that both load and velocity affect the wear performance, and their critical loads and sliding velocities (where wear volume and wear rate are minimum) were found to be 10 N and 1 m/s, respectively. In the same study, the average CoF's were in the range of 0.35-0.45, but higher values (0.5-0.7) were obtained at lower loads (≈5 N). Parler et al. [21] also concluded that Zr-based BMGs exhibit better tribological behavior than many 'conventional' materials such as AISI 304 under similar conditions. Zhou et al. [22] has reported the effect of Fe addition on the thermal, mechanical, and tribological properties of Zr-Cu-Ni-Al-based bulk metallic glasses. The formation of second glassy phase was confirmed by the TEM analysis, which results in multiple shear bands, enhanced toughness and oxidative wear that enhances the wear resistance of Zr-Cu-Ni-Al BMGs.

For BMGs, their structure and properties depend not only on composition but also on the processing conditions and level of stress relaxation they have been exposed to before the experiments. In this context, an important parameter known as 'fictive temperature' $T_{\rm f}$, is utilized which is defined as the temperature where a supercooled liquid deviates from the metastable state. A sample described by a certain T_f is reflecting the same structural state that the sample features at that temperature when it is fully relaxed. Thus, different $T_{\rm f}$'s define different structural states, reflecting different degrees of relaxation that the BMG samples have undergone [23-25]. Since every distinct structural state has a specific set of properties associated with it, any change in T_f will lead to a change in the material's mechanical as well as tribological behavior. As a consequence, the influence of different thermal treatments on the structure of BMG's and properties like density [26,27], elastic modulus [28-30], and plasticity [31,32] due to changes in the structural relaxation and the formation of short-range ordered structures

have already been studied. Previous researchers have reported the effect of the fictive temperature on the bulk mechanical properties (microhardness, elastic modulus, yield strength, and fracture toughness) of $Zr_{44}Ti_{11}Cu_{10}Ni_{10}Be_{25}$ metallic glass, and found that with increased $T_{\rm f}$ mechanical properties deteoriorated [33,34]. This trend can be understood by noting that lower $T_{\rm f}$'s mean annihilation of more free volume from the material which results in the formation of denser randomly packed atomic structure. This dense structure impedes plastic flow of atoms and thereby results in enhanced mechanical performance [33].

More generally, due to the importance of understanding the effect of processing on structure, a large number of previous researches have been dedicated to gain insight into this relationship by studying physical (e.g., enthalpy changes, density, etc.), mechanical (hardness, modulus, etc.) or tribological properties, the latter of which were mainly focused exploring the effect of different sliding conditions on wear resistance [19–21,35–37]. However, most of these existing studies used heuristic annealing protocols, rendering the material's mechanical properties not completely reproducible, preventing further systematic analysis. To overcome this deficiency, this work studies the tribological properties (i. e., scratch and wear) of Zr₄₄Ti₁₁Cu₁₀Ni₁₀Be₂₅ metallic glasses as a function of their different fictive temperatures and corresponding distinct structural states and BMG with fictive temperature 320 °C is found to be most wear resistant. Since these states are expected to be fully reproducible, the results reported in this work can potentially open a pathway towards creating a toolbox for tailoring a glass' tribological properties for applications that include mechanical devices such as ultra-fine gears, coatings in dry bearing in space [38]. More recently there has been a lot of interest in nanostructured surface texturing of these BMGs using nanoimprinting techniques [39-41] for applications like photonic devices [42], fuel cell electrodes [43], water filtration [44], anti-friction surfaces, etc. Understanding the influence of structural manipulation using fictive temperature processing on the tribological properties of BMGs is therefore of great importance in future BMG applications.

2. Materials and methods

2.1. Processing of BMGs

Zr₄₄Ti₁₁Cu₁₀Ni₁₀Be₂₅ bulk metallic glass (BMG) was purchased from Materion (Mayfields Heights, Ohio). This as-cast BMG material was first thermoplastically formed using a modified Instron mechanical tester to reduce casting flaws by heating at 420 °C (above T_g) for 2 min at the load of 1 kN followed by rapid quenching in distilled water. The samples were then processed (annealed) to obtain the structural state defined by three different fictive temperatures T_f 's (320 °C, 350 °C, and 370 °C). Upon annealing the sample at a fixed temperature T, the bulk metallic glasses go through various stages of structural evolution until it is treated to the time longer than its relaxation time where the structure gets fully relaxed. The relaxation time (τ) for the bulk metallic glasses at a temperature (T) is defined by the Vogel-Fulcher-Tammann [45,46] relationship which is mentioned below in eq (1):

$$\tau(T) = \tau_0 exp\left(\frac{D^* T_0}{T - T_0}\right) \tag{1}$$

where τ_0 is the relaxation time at very high temperature (at $T\to\infty$, $\tau_0=2.5\times 10^{-13}$ s for Zr based bulk metallic glasses [47]). D° is the constant referred as fragility parameter whose value is equal to 28.13 [48]. From the expression it is clear that the relaxation time varies exponentially with the fictive temperature and these values are reported in Table 1, the annealing time required to achieve relaxation at fictive temperature of 300 °C i.e. $0.85T_g$, would be 186 h which increases to 455 days for fictive temperature of $0.8T_g$ i.e. 280 °C, and to several millennia for the fictive temperature of $0.6T_g$. Therefore, for the experimental feasibility the starting fictive temperature are chosen to be $0.91T_g$ which requires

Table 1 Fictive temperatures and nomenclature of the BMG samples used in this study, where $T_{\rm f}$, $T_{\rm g}$, $t_{\rm relax}$ and $t_{\rm crystal}$ represent a sample's fictive temperature, glass transition temperature, relaxation time, and crystallization time respectively.

Nomenclature	T_{f} (°C)	T _g (°C) [45]	$t_{ m relax}$	t _{crystal} [47,51]	$T_{\rm f}/T_{\rm g}$	% Crystallinity
As-cast	-	352	_	_	1.1	6.5
BMG370	370	352	\approx 32 s	$\sim \! 100 \; min$	1.05	8.6
BMG350	350	352	${\approx}350~\text{s}$	_	0.99	8.9
BMG320	320	352	>6 h	>10 years	0.91	8.9

around 6 h (Table 1) of annealing to attain. Annealing of the samples was carried out in a furnace with heating rate of 20 °C/min until the target temperature was reached, and then the samples were held at that temperature for a duration larger than 1.5 times of the relaxation time characterized by its T_f but significantly less than the time at which an onset of crystallization could be detected. Crystallization time calculated by the differential thermal scanning for Zr based bulk metallic glasses is also mentioned in Table 1. A detailed description of how fictive temperature processing of BMGs is carried out has also been reported in the recent work [33]. The longer duration for crystallization (Table 1) restricted the full crystallization of BMGs with fictive temperature of 320 °C (0.91 T_g) and 350 °C (1.05 T_g) and therefore in this study, only the sample with fictive temperature of 370 °C is further annealed for a duration exceeding the time for full crystallization. Samples were then cut by using a low-speed diamond saw and coarse polished by using abrasive papers of grit size 1200-2500, followed by cloth polishing (MicroCloth, Buehler) using 0.1 µm diamond paste to achieve the mirror finish required for micro-scratch testing (sample roughness was 30-60 nm). Amorphous and crystalline state of the metallic glasses annealed at different fictive temperatures, was confirmed via X-ray diffraction (Appendix A1, for fully crystallized sample) performed with a Rigaku Miniflex 600 Two Circle diffractometer (Cu K α radiation, $\lambda = 1.5406$ Å) in a 2θ range between 20° and 80° with scan rate of $5^\circ/min.$ Differential scanning calorimetry (DSC, STA8000, PerkinElmer, USA) of the BMGs was further done in the inert Ar gas environment with heating rate of 20K/min to confirm the thermal state of sample. DSC has also been utilized by various researchers [49,50] to calculate the percentage crystallinity as the ratio of enthalpy for sample to 100% crystalline material, but in the present work no sample has shown the 100% crystalline nature and therefore it could not be used. However, the XRD pattern was further used to calculate the percentage of crystallinity (Table 1) despite of moderate error associated with this method. The Zr-BMG samples with different fictive temperatures used in this research along with their nomenclature are listed in Table 1. As-cast bulk metallic glasses are assumed to have $T_{\rm f}/T_{\rm g}$ equal to 1.1.

2.2. Mechanical properties

Hardness and effective elastic moduli of the BMGs are calculated using nanoindentation on a TI750 Hysitron Ltd. machine. At least 15 indents were performed on each sample, with a maximum load of 8000 μN and a loading rate of 2500 $\mu N/s$. A diamond Berkovich indenter tip (Bruker India Scientific Pvt. Ltd.) with a radius of 150 nm, Poisson ratio of 0.07, and elastic modulus of 1141 GPa [52] was used to perform the indents. Contact area calibration was done before the experiments by using standard fused silica with a hardness of 9.25 GPa and an elastic modulus of 69.6 GPa. The experiments were carried out using the continuous stiffness measurement method [52], which results in the estimation of hardness and effective modulus as a function of penetration depth. During nanoindentation, the two solid surfaces come in contact and therefore the contact stiffness between the indenter and surface is given by the following equation [53]:

$$S = \frac{dP}{dh} = 2E_r \sqrt{\frac{A}{\pi}} \tag{2}$$

where *P* 00204075, *h* the penetration depth, and *A* the area. $E_r = ((1 - \nu_s^2)/E_s) + ((1 - \nu_i^2)/E_i)^{-1}$ is the reduced modulus that is related to the effective modulus of indenter and specimen, by using Young's modulus and Poisson's ratio of the indenter material ($E_i = 1141$ GPa, $\nu_i = 0.07$ for diamond) and the sample (E_s , ν_s), respectively.

In the case of elastically isotropic materials, their effective modulus can be obtained with the following equation:

$$E_{eff}^{s} = \frac{E_s}{(1 - \nu_z^2)} \tag{3}$$

From the load versus displacement curves, the elastic energy $W_{\rm e}$ (i.e., the elastic work done during the indent) is calculated as the area under the unloading curve, whereas the total energy $W_{\rm t}$ is determined from the area under the loading curve. Plastic work or irreversible energy $W_{\rm p}$ is calculated as $W_{\rm p}=W_{\rm t}$ - $W_{\rm e}$. On this basis, the plastic energy to total energy ratio (PE/TE) is also calculated for all the samples to represent the effect of fictive temperature on plasticity.

2.3. Scratch resistance at constant and progressive loading

The effect of $T_{\rm f}$ on damage tolerance and damage initiation in the BMGs was studied by micro-scratch testing under constant and progressive loading conditions with three scratches performed on each sample. The scratch test was carried out using a micro-scratch tester (MHT, CSM Instruments, Switzerland). A Rockwell diamond indenter with a radius of 0.1 mm was used to create a scratch of length 1 mm at a constant load (10 N, 0.2 mm/min indenter speed) and progressive load (0.5–25 N, loading rate 5 N/min). The coefficient of friction (CoF) and penetration depth d were continuously recorded during scratching. The wear volume (W_{VS}) was then calculated using the following equation:

$$W_{vs} = AL \tag{4}$$

where L is the length of the scratch and A it's cross-sectional area that was obtained from [54].

$$A = R^{2} cos^{-1} \left[1 - \frac{d}{R} \right] - \left(R - d\sqrt{2Rd - d^{2}} \right)$$
 (5)

with R being the radius of the indenter (0.1 mm) and d is the penetration depth during scratching.

Cross-sectional depth profiling of the constant-load scratches has been carried out at different locations of each scratch to observe the penetration depth and extent of pile-up in the samples. This depth profiling was done by using an Optical Profilometer (Zegage optical surface profilometer, Zemetrics). Furthermore, the pile-up area for each location in all scratches is calculated by the area under the curve of the corresponding peak using Origin Software (OriginLab Corporation, USA). Average values of these areas are then reported to enable a comparison of material removal during scratching among all tested samples. Acoustic emission data recorded during progressive scratching, was also utilized to determine the critical loads $F_{\rm c}$ at which crack initiation and crack propagation occurs in the material.

Scratch testing has also been utilized to evaluate the mechanical properties of BMGs. For example, the scratch hardness H_s is defined as [55]:

$$H_{\rm s} = \frac{8F}{\pi w^2} \tag{6}$$

where F represents the normal load (taken as 10 N for constant loading and as 25 N for progressive-load scratching, reflecting the maximum load during the test) and w denotes the scratch width that has been measured from SEM micrographs of scratch traces using the ImageJ software [54]. Similarly, the scratch fracture toughness K_S was also calculated by using the force applied during scratching and the indenter geometry using the following relation [55].

$$K_{\rm S} \propto \frac{F_T}{4\left[\frac{1}{3}\beta\left(\frac{d}{R}\right)\right]^{\frac{1}{2}}dR^{\frac{1}{2}}} \tag{7}$$

where $F_{\rm T}$ is the tangential force, d the penetration depth, β is the dimensionless parameter and R the radius of the indenter (i.e., $100~\mu m$). However, to determine $K_{\rm S}$, the indenter shape function f and its variation with depth d are required. For a spherical probe, f is defined by the following two equations:

$$f = 2p(d)A(d) \tag{8}$$

$$f(d) = \frac{16}{3}\beta \left(\frac{d}{R}\right)d^2R \tag{9}$$

where *A* is the contact area and *p* is the perimeter of indenter. After calibrating the indenter shape function, $2\rho A$ was found to be equal to. $13.02(d)^3$.

Therefore, the scratch fracture toughness was estimated from the following equation [55]:

$$K_{\rm S} = \frac{F_{\rm T}}{(2pA)^{1/2}} \tag{10}$$

From Equation (10), the slope of the plot between F_T^2/R^3 and $2pA/R^3$ gives the value of fracture toughness K_S .

3. Results and discussion

3.1. Structure and thermal behavior

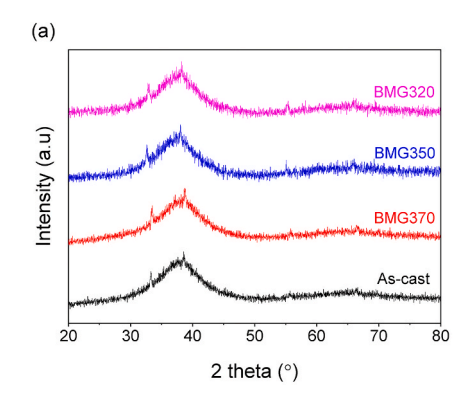
Amorphous state of the Zr based bulk metallic glasses are confirmed by the XRD spectra (Fig. 1(a)) with the presence of broad single peak which is in accordance with the work reported previously [33]. However, in the present work, a peak of unknown phase is present around the 2θ value of 32° which represents that there might be some intermetallic formation during annealing or those might be some background noise obtained during scan. Assuming those peaks to be of some crystalline phase, percentage of crystallinity of all the metallic glasses was calculated by using area under the curve of XRD pattern and the values are listed in Table 1. The values associated with this measurement method are very rough with higher error, therefore these might be insignificant. However, the values reported in Table 1 indicate that there might be some crystalline phase present in the as-cast BMGs and that phase is retained even after the annealing of BMGs at different fictive temperatures. XRD pattern also indicates that no new crystalline phase formation has occurred during annealing of BMGs at the desired fictive temperature. For the fully crystallized sample, XRD pattern (Appendix A1) reveals the presence of various peaks of Ni₂Zr₃ which

also confirms the crystalline nature of the same.

Differential Scanning Calorimetry results of different BMGs are shown in Fig. 1(b), where it is clearly visible that the heat flux of BMGs is higher for low T_f which indicates more structural relaxation at lower fictive temperature ($T_{\rm f}$ - 320 °C). Presence of glass transition ($T_{\rm g}$), crystallization peak (T_x) confirms the glassy state of all the BMGs. DSC curve further indicates that there might not be sufficient crystallinity in the samples as glass transition temperature is same as of the fully amorphous metallic glasses. Same conclusions have already been drawn from the XRD analysis as discussed before. For fully crystallized material (Fig. A1) there is no crystallization peak present which confirms the samples were almost fully crystallized. During processing of metallic glasses, fast cooling/quenching leads to the generation of various defects like stress inhomogeneities, shear transformation zones, free volume etc. The extent of free volume entrapped within the material depends on the relaxation time and it affects their mechanical, physical and tribological properties, therefore it becomes important to understand the degree of free volume annihilation/removal during processing of BMGs at different fictive temperatures. Evenson et al. [56] Slipenyuk et al. [57] and Haruyama et al. [58] have reported the correlation between the free volume and enthalpy. Accordingly, the enthalpy recovered from the bulk metallic glasses with lower fictive temperature need to be higher than the bulk metallic glasses with higher fictive temperature ($T_f = 350$ and 370 °C) which is also observed in the present study (inset in Fig. 1 (b)). Therefore, it can be concluded that BMGs annealed at lower fictive temperature ($T_{\rm f}=320~^{\circ}{\rm C}$) are structurally more relaxed than the BMGs annealed at higher fictive temperature ($T_{\rm f} = 350\,^{\circ}{\rm C}$ and $370\,^{\circ}{\rm C}$) which is in accordance with the previous work [33]. At lower fictive temperature, more annihilation of free volume due to lower thermal energy is the possible reason for higher structural relaxation of BMGs resulting in the formation of dense randomly packed structure. In the next section, effect of structural relaxation on the hardness and elastic modulus are discussed and from the above discussion it is expected that structural relaxation will enhance the mechanical behavior due to restricted movement of shear bands.

3.2. Mechanical behavior

Fig. 2(a) represents the load vs. displacement curves obtained during nanoindentation of the bulk metallic glasses annealed at different fictive temperature. From the figure it can be observed that the penetration depth (i.e., the displacement of the indenter tip into surface) obtained increases for higher T_f 's. This can easily be understood considering that previous research [33,34] has shown that annealing of metallic glasses at a fixed temperature enables a structural relaxation, which leads to a reduction in free volume or, in other words, an increase in density. Once the material has been kept for certain period of time at that temperature, the material is considered to be 'fully relaxed', meaning that heated for even longer, only minimal decreases in the free volume/increases in



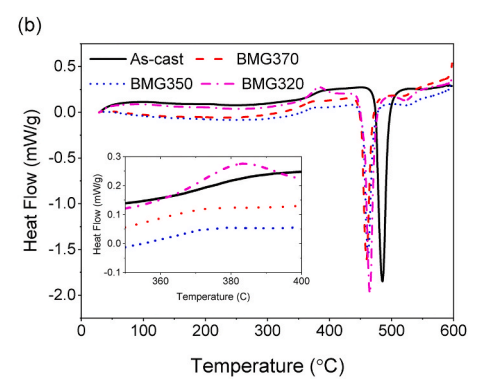


Fig. 1. (a) XRD patterns of the metallic glasses heat treated at different fictive temperature. The nomenclature is defined in Table 1, (b) DSC thermograms of Zr -BMG samples heat treated at different fictive temperatures, inset figure enlarges the glass transition region where the glasses relax freely.

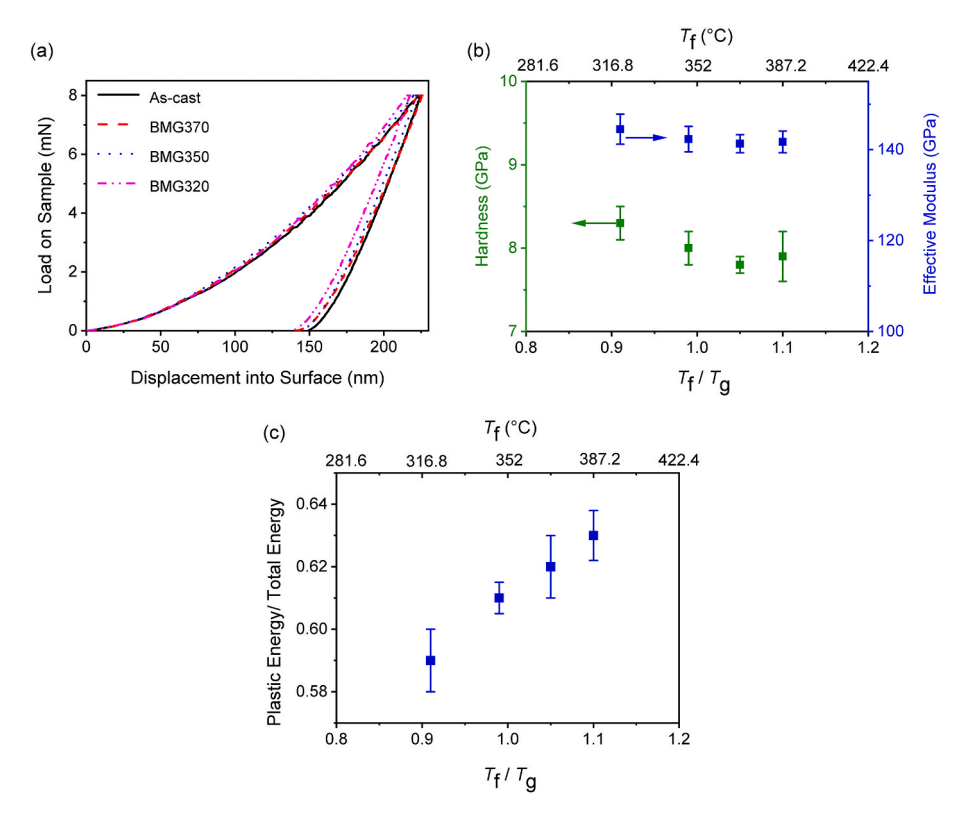


Fig. 2. Berkovich nanoindentation experiments on metallic glasses with different T_f (a) Load on sample versus displacement into surface representative curves. (b) Average hardness (green) and effective elastic modulus (blue) plotted as a function of the T_f . (c) Variation of the plastic energy over total energy ratio (PE/TE) for the same BMG samples. (For interpretation of the references to color in this figure legend, the reader is referred to the Web version of this article.)

density are being observed. Since the highest density that can be achieved when annealing at a specific temperature without crystallizing the sample is a fixed, reproducible value, the structural state equivalent to that density can be assumed as fully reproducible and described by the temperature at which the annealing took place, which is then referred to as the above-mentioned 'fictive temperature' $T_{\rm f}$. At lower $T_{\rm f}$'s, the atoms are closer when being fully relaxed which increases the density of samples due to increased short range ordering and a reduction of free volumes. This increased density and reduced free volume, impedes the displacement/flow of atoms, thus affecting the mechanical properties. Based on it, penetration depth during indentation increases as the $T_{\rm f}$ increases from 320 °C to 370 °C.

Hardness and effective elastic modulus calculated from the load vs. displacement curves of the bulk metallic glasses annealed at different fictive temperatures, are shown in Fig. 2(b). Thereby, the penetration depth at peak load is used to calculate the hardness whereas the effective elastic modulus is calculated by utilizing the slope of unloading curve of load versus displacement plot. As expected, out of all tested samples, the hardness is observed to be the highest for the BMG with $T_{\rm f}=320$ i.e. 8.4 \pm 0.2 GPa, followed by metallic glasses with fictive temperature of 350 °C and 370 °C with hardness values of, 7.9 \pm 0.1 GPa, and 7.8 \pm 0.1 GPa, respectively. The effective elastic moduli of these metallic glasses are 144.5 \pm 3.3 GPa, 142.3 \pm 2.8 GPa, and 141.4 \pm 2.0 GPa, respectively for BMG320, BMG350, and BMG370. The as-cast bulk metallic glass exhibits hardness and effective elastic modulus of 7.9 \pm 0.3 GPa and 141.7 \pm 2.5 GPa, respectively, which is consistent with the expectation that it would be close in properties to a sample with $T_{\rm f}=370$ °C.

Fig. 2(c) finally represents the variation of the plastic energy to total energy ratio (PE/TE ratio) for the different samples, with PE/TE ratio for the fully crystalline sample again shown in Appendix A1. The 'plastic energy', which reflects the work done during indentation that is not recovered during retraction, measures the extent of bond breakage or permanent deformation in the material [59]. Higher PE/TE ratio

indicates more plastic deformation or penetration depth during indentation. From the figure, it is clear that the PE/TE ratio is minimum for BMG320 (i.e., 0.58) followed by BMG350 (0.60), BMG370 (0.62), and as-cast (0.63) BMGs, which indicates the highest structural stability of BMG320 as compared to other BMGs. As fictive temperature increases from 320 °C to 370 °C, free volume entrapment in the structure and long-range ordering increases lead to the enhanced value of plastic energy ratio or plastic deformation in the material. Interestingly, the fully crystallized sample (Table A1) shows the highest PE/TE ratio (0.64), which indicates a higher level of plastic deformation in the sample compared to the others. The presence of long-range ordering, which leads to the formation of localized dislocations, presence of more glide planes in the crystal structure, and other defects might be the possible reason for the higher PE/TE ratio or plasticity of the fully crystallized sample.

Hardness and the effective elastic modulus increase with a decrease in fictive temperature primarily because of the increased density, increased short range order and reduced percentage free volume in the sample leading to increased resistance to atomic flow, shear band movements and plastic deformation. From the above section it can be concluded that BMG320 is exhibiting highest hardness and elastic modulus due to higher level of structural relaxation and highly dense randomly packed structure. The effect of fictive temperature on the damage tolerance of bulk metallic glasses during micro-scratch testing at constant and progressive loading conditions is discussed in the following sections and based on the hardness and effective elastic modulus values; it is expected that the scratch resistance of Zr based bulk metallic glasses will decrease with increase in the fictive temperature.

3.3. Micro-scratch at constant load

Steady-state damage tolerance of BMG samples was evaluated using constant load scratch testing. Fig. 3(a) represents the variation of the

coefficient of friction (CoF) with the scratch length for micro-scratching carried out at a constant load of 10 N. From the Fig. 3(a), it can be observed that CoF values are quite similar for all BMGs, and it is minimum for BMG350. From the CoF plot, CoF first increases sharply but then decreases and later becomes constant, as shown in the circle. This phenomenon is known as the "running-in" period, in which the wear rate is usually higher. However, it is always to be expected in these experiments as when the sample and the indenter first come into contact, changes in the topography of the initial surface, oxidation or changes of phase induced by surface deformation etc., may occur, which increases the CoF sharply [11]. However, after some duration, oxide/contaminations present on the surface may get worn or some new film may get formed that decreases the CoF and makes it almost constant. This duration of constant CoF is termed as steady state [60].

For further analysis of the scratch, pile-up areas/cross-sectional depth profiles associated with the scratches, penetration depths, scratch widths, wear volumes, and wear rates for all the samples studied in this work are represented in Fig. 3(b)-(d). All of these parameters are important factors when attempting to assess the wear behavior and are found to be lowest for $T_{\rm f}=320~{\rm ^{\circ}C}$. BMGs undergo plastic deformation during scratch testing, which leads to material removal from the surface that usually gets piled up at the edge of the scratch. The volume of this 'pile-up material' can be utilized to determine the extent of material removal or wear of the material. This pile-up area is determined by taking the cross-sectional profile at multiple locations of each scratch and then averaged. Fig. 3(b) shows the cross-sectional depth profile at 10 N load post scratch testing, and the extent of material pile-up in the samples is calculated by area under the peak. The pile-up material area is minimum for BMG320 (i.e., \sim 18 μ m²), increasing to approximately 27 μm^2 and 30 μm^2 respectively for BMG350 and BMG370. The as-cast BMG shows a pile-up area of \approx 19 μ m². Reduced hardness and increased plasticity with increased fictive temperature are the main reason behind the higher pile-up of material as $T_{\rm f}$ increases. The fully crystallized material has shown (Table A2) the highest pile-up area $(\sim 32 \mu m^2)$, possibly due to the higher extent of plastic deformation as shown previously by higher PE/TE ratio.

Penetration depth values obtained during scratch at a load of 10 N increase from 1.5 \pm 0.3 μm for BMG320 to 1.6 \pm 0.2 μm and 1.8 \pm 0.3 μm for BMG 350 and BMG370 and finally the maximum value of 2.1 \pm 0.2 µm for the as-cast sample. Similarly, the scratch widths, wear volumes and wear rates also follow the same trend with maximum values for, e.g., as-cast BMG and BMG370 scratch widths being 57 \pm 1.3 μm , followed by BMG350 (55 \pm 0.7 $\mu m)$ and minimal for BMG320 (49 \pm 0.9 μm). Similarly, wear volumes and wear rates were the highest for as-cast metallic glasses (3.7 \times 10⁻⁵ mm³ and 3.7 \times 10⁻³ mm³/Nm, respectively) and minimal for BMG320 (1.5 \times 10⁻⁵ mm³ and 1.5 \times 10⁻³ mm³/ Nm). This behavior can be easily understood considering that as $T_{\rm f}$ increases from 320 $^{\circ}\text{C}$ to 370 $^{\circ}\text{C},$ a decrease in hardness, as discussed in previous sections, directly results in a deterioration of the material's wear performance. It is worthy to note here that as the fictive temperature increases above the glass transition temperature (352 °C for the Zrbased metallic glass used in this study), the mode of deformation changes from brittle to ductile [34]. Therefore, at lower $T_{\rm f}$, metallic glasses undergo brittle fracture; thus the extent of deformation is less but as T_f reaches close to T_g , plasticity in the metallic glasses increases which leads to enhanced plastic deformation and deteriorates wear performance of the bulk metallic glasses. In the case of the fully crystalline sample, the long-range atomic ordering further promotes the formation of defects such as dislocations etc., that trigger increased plastic deformation resulting in higher wear volume and wear rate [20].

3.3.1. Analysis of worn surfaces

To establish the wear mechanism, SEM micrographs of the worn surface of the BMGs are examined and shown in Fig. 4(a–l). The presence of linear long parallel grooves in the center of the scratch traces of all the samples confirms the mechanism to abrasive wear [19,61]. The presence of shear bands at the edge of scratch traces is also visible, following the previous studies [19,62]. During scratch testing at constant load, SEM micrographs reveals the presence of shear bands as well as micro-cracks at the edge of worn-out surfaces. With the application of load during scratch testing, BMGs undergo shear deformation and form residues, which causes the material to experience additional friction

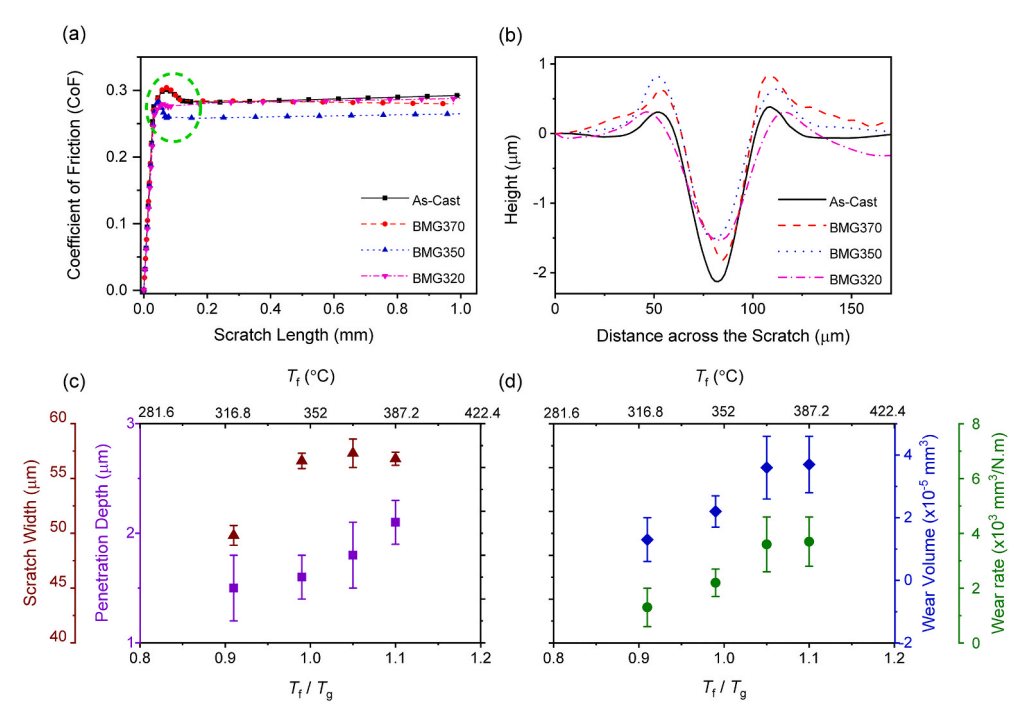


Fig. 3. Results from micro-scratch experiments performed at constant load. (a) Variations of the coefficients of friction as they occur with scratch length; (b) Cross-sectional depth profiles of the scratches, which are used to get an estimate of the pile-up area; (c) Scratch widths and penetration depths; and (d) Wear volumes and wear rates. As before, data points in panels (c) and (d) are plotted as a function of their fictive temperature.

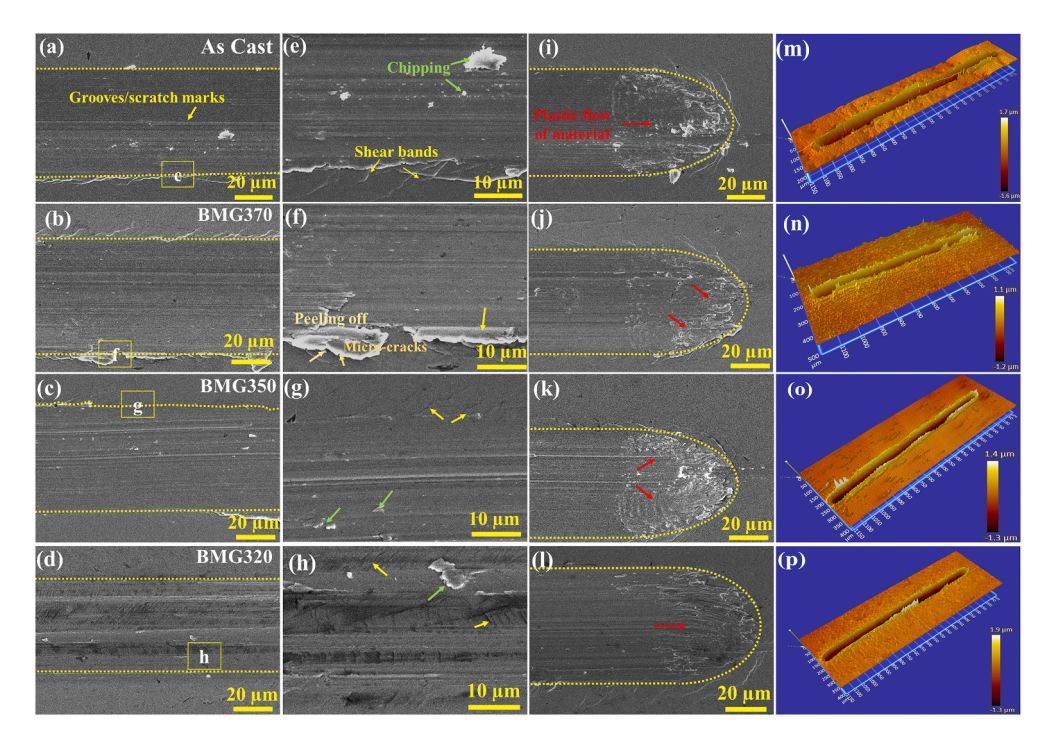


Fig. 4. (a–l) SEM micrographs of scratches at the surfaces of BMGs taken to reveal the presence of cracks, delamination fracture, etc. in the scratch traces. (m–p) Optical profilometry images of the scratch grooves used to characterize the penetration depth, shape of the scratch profile, and the degree to which pile-up occurs at the edges.

along with material removal from the surface [63]. Plastic deformation causes the material to pile-up at the edge of the scratch grooves experiencing tensile stresses while loading. These stresses result in micro-crack formation (Fig. 4(f)) at the edge of the tracks. Formation of the cracks in the direction perpendicular to the scratch direction indicates the brittleness of Zr-based BMGs. Linear grooves, micro-cracks, plastic viscous flow, and peeling off of the material are clearly visible in all the BMGs; however, their extent is varying with the fictive temperature. In BMGs, as the T_f increases, the extent of both the micro-crack formation and shear bands and plastic flow of material increases (highlighted by red arrows in Fig. 4(i and j)), resulting in a reduced wear resistance for metallic glasses with higher $T_{\rm f}$. The existence of a reduced amount of plastic deformation and cracks in BMGs with $T_{\rm f}=320~^{\circ}{\rm C}$ (Fig. 4(f) and (j)) as compared to other BMGs are indicative of its superior wear resistance due to increased structural relaxation, density and hardness. It is worthy to note here that the interspacing between the grooves increases with $T_{\rm f}$. In the metallic glasses, abrasive wear along with the shear band formation due to inhomogeneous deformation is the dominant wear mechanism. However, for the fully crystalline sample (Fig. A2), dislocation motion-induced plastic deformation is the dominant wear mechanism that leads to more material loss and thus lowers wear resistance as compared to the metallic glasses. Optical profilometry of the scratches has been done to observe the scratch grooves shape, penetration depth, and pile-up of the material, and the images are shown in Fig. 4(m-p).

Optical profilometry images represent the depth profile of the scratches performed on the BMGs and the penetration depth values are following the values reported in Fig. 3(c). Pile up of the material at the scratch traces is also visible via these profilometry images which indicates that the extent of pile up of removed material at the edge of scratch traces is minimum for BMG320 that makes it to be the more damage tolerant metallic glass at load of 10 N among all the metallic glasses discussed in the present work.

EDX analysis of the worn surface of as-cast bulk metallic glass after scratching at load of 10 N (Fig. 5(a)), reveals the presence of Zr, Ti, Ni, Cu and Be elements (Fig. 5(b)) which belongs to the parent glass matrix.

Thus, it can be concluded that during scratch testing of the metallic glasses, no new phase/tribo-layer formation has occurred.

There are certain applications which involve a continuous increase in the load during service. Therefore, in such cases it becomes mandatory to study the loads at which damage initiates and its mechanism in the metallic glasses during service conditions. Such study is carried out by scratching under progressive loading conditions which is discussed in the next section.

3.4. Micro-scratch formation during progressive loading

The results from scratch testing at a constant load of 10 N presented in the previous section revealed that the BMG with $T_{\rm f}=320~{\rm ^{\circ}C}$ is the most wear-resistant of all metallic glass samples analyzed in this work. This section now focuses on scratch testing at progressive loading conditions to estimate the load necessary to initiate and propagate cracks in the metallic glasses. Fig. 6(a) and (b) represent the variation of the coefficient of friction (CoF) and the penetration depth with increasing load and scratch length, respectively. For all metallic glasses tested, both the CoF and the penetration depth increase linearly with the applied load. In agreement with findings from the previous section, penetration depth was found to be highest for BMG370 and lowest for BMG320.

Fig. 6 (c) and (d) disclose the wear properties of the metallic glass samples for progressive loading tests. Penetration depth, wear volume and wear rate are minimal for BMG320 followed by the as-cast metallic glass. More specifically, the penetration depth for BMG320 is $15\pm2.1~\mu m$ but increases to $17.9\pm2.8~\mu m$ for as-cast BMG, $23.5\pm1.1~\mu m$ for BMG350, and $28.3\pm1.6~\mu m$ for BMG370, respectively. Next, the increased indentation hardness with annealing at lower fictive temperature (7.8 GPa for BMG370 to 8.4 GPa for BMG320; see Fig. 2(b)) resulted in a decreased penetration depth for BMG320 compared to the other samples. Finally, the scratch width at maximum load (i.e, 25 N) also follows the same trend with being minimal for the metallic glass with a fictive temperature of 320 °C (i.e., $81\pm0.7~\mu m$), followed by 92 $\pm0.6~\mu m$ for BMG350, $93\pm0.9~\mu m$ for BMG370, and $95\pm0.7~\mu m$ for the as-cast bulk metallic glass.

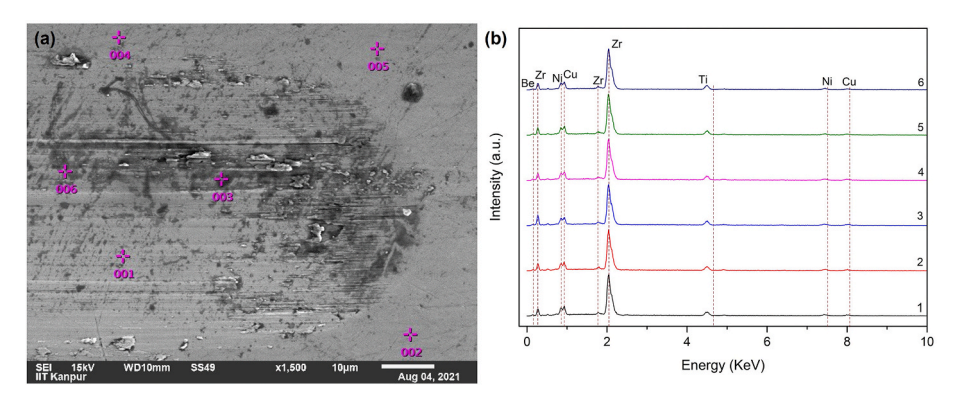


Fig. 5. Elemental analysis of the wear surface (a) SEM image of scratched surface (b) Chemical analysis of the scratched surface.

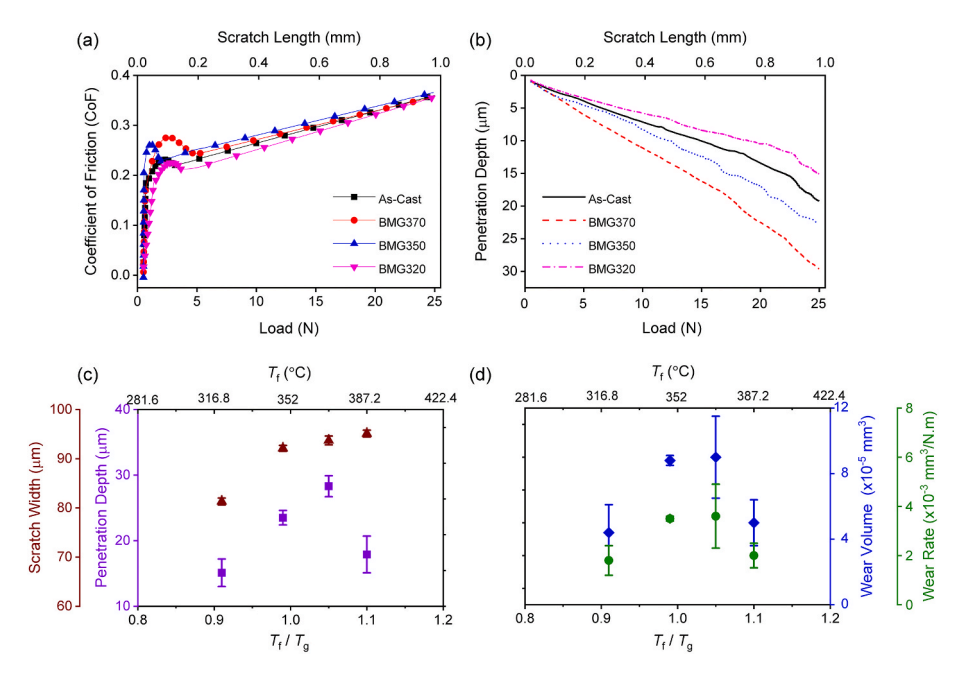


Fig. 6. Representative curves for (a) The coefficient of friction and (b) The variation of the penetration depth during progressive loading for all samples tested. (c) Penetration depths and scratch widths and (d) Wear volumes and wear rates obtained during progressive scratching, with their values taken at the highest load applied during each scratch (i.e., 25 N).

Overall, BMG320 is again found to be most wear-resistant, featuring the lowest wear volume (4.4 \times 10^{-5} mm^3) and wear rate (1.8 \times 10^{-3} mm^3/Nm), respectively. The wear volume increases to 5.0 \times 10^{-5} mm^3 for as-cast BMG, 8.8 \times 10^{-5} mm^3 for BMG350, and 9.7 \times 10^{-5} mm^3 for BMG370 respectively. The wear rate follows a similar trend as the wear volume, being minimal for BMG320 (1.8 \times 10^{-3} mm^3/Nm) and maximum for BMG370 (3.6 \times 10^{-3} mm^3/Nm).

When as-cast bulk metallic glasses are annealed at fictive temperature of 320 °C, the resulting increased hardness and higher elastic modulus (Fig. 2) lead to a 10% increase in wear resistance due to increased short-range order and more annihilation of free volumes in the BMGs as the fictive temperature decreases. Conversely, higher $T_{\rm f}$'s cause lower hardness, increased plasticity, more free volume, and reduced ordering, resulting in decreased wear resistance (by 75% when comparing BMGs with $T_{\rm f}=350~^{\circ}{\rm C}$ and 370 °C to as-cast glasses. Therefore, based on the progressive load wear testing results, the BMG with $T_{\rm f}=320~^{\circ}{\rm C}$ is observed to be most damage-tolerant compared to all other samples analyzed.

Acoustic emission (AE) data was recorded during the progressive load test to detect cohesive failure events such as cracks initiation, crack propagation, etc. In metallic glasses, the generation of AE signal spikes or sharp peaks of AE signals represents the critical loads at which crack initiation, propagation, spallation, and other events occur [24]. Formation of the cracks, delamination, or different mode of fracture in the material release more energy, and thus, AE signals are generated. Fig. 7 represents the AE data for the progressive load and scratch length. In the case of as-cast metallic glasses, a sharp peak is observed to be present at a load of \approx 24 N, which might be due to crack initiation at the surface during scratch. However, there is no evidence of crack formation in BMG320 that can also be confirmed via SEM micrographs (Fig. 8). Structural relaxation in the metallic glass has led to enhanced hardness and resistance to deformation in the BMG320. Therefore, no crack formation has occurred in this load range and thus, AE signals are not present [37]. In the case of BMG350 and BMG370, small peaks are present that may represent the formation of the micro-cracks in the scratch.

Fig. 8 shows representative SEM micrographs of the scratch traces on the various BMG samples after scratch testing under progressive loading condition. SEM images reveal the presence of shear bands, ploughing, cracks, viscous flow, and chipping for all samples. The wear mechanisms are abrasive wear and plastic deformation due to cracks, shear bands, and ploughed material, respectively, at the edges and the ends of the scratch traces. The extent of plastic deformation (or plastic flow of material) is minimal for BMG320 and increases for higher T_f 's due to the

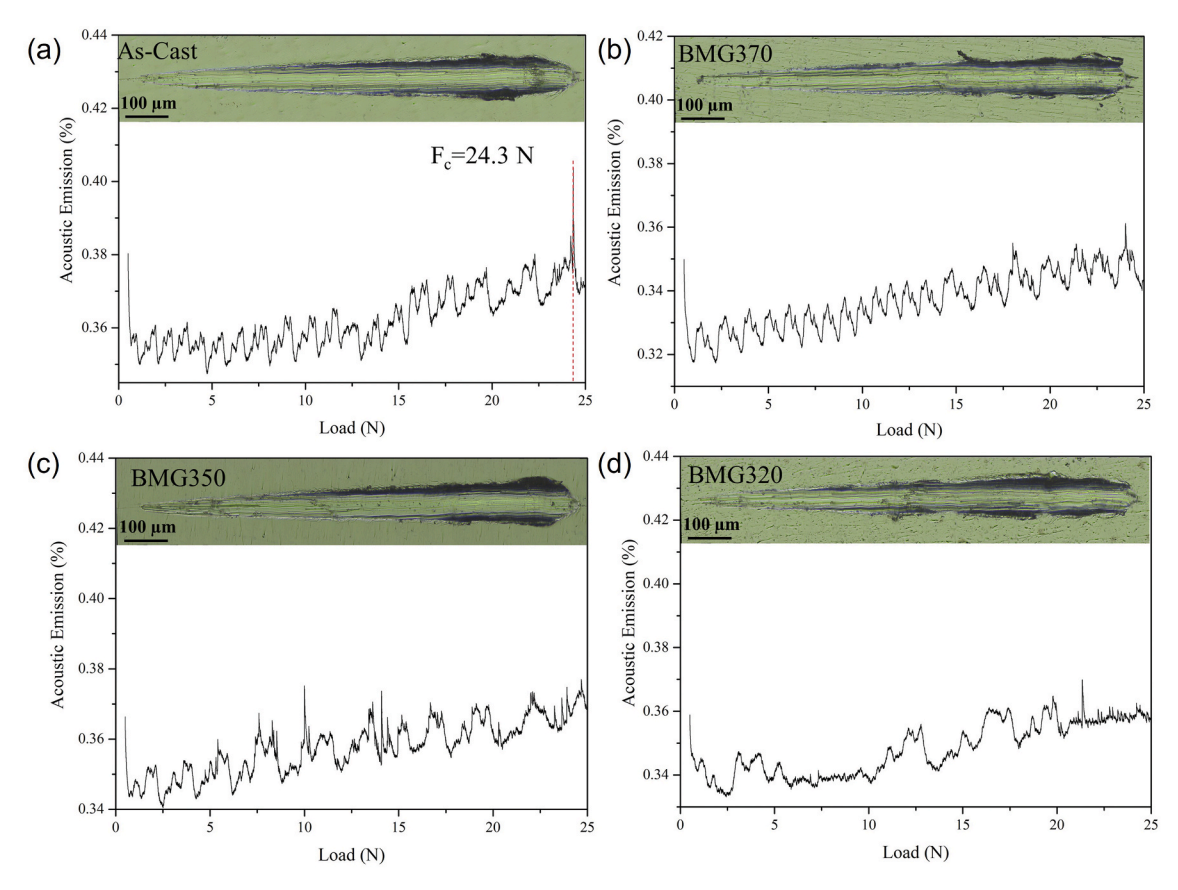


Fig. 7. Acoustic emission (AE) of the metallic glasses during scratch testing at progressively increasing load. Optical micrographs of the scratch traces are shown in the insets at the top, representing the start and end points of the trace (Total time taken to perform the scratch is 5 min).

earlier-discussed fact that the additional available free volume facilitates plastic flow, similar to the behavior observed during the constant-loading experiments (Fig. 4). It is important to note that during progressive loading, the interspacing of grooves increases with load, which is also visible in the microstructure. Shear band formation, which represents an abrasive wear mechanism, is observed to be present in the scratch traces and is minimal for BMG350 and BMG320 due to their nearly equal plasticity energy ratio. Shear band formation further increases with increase in the fictive temperature as shown for BMG370 and as-cast BMG.

3.5. Validation of the Archard's law

Structural relaxation in the bulk metallic glasses leads to changes in the mechanical and physical, mechanical and wear properties. In case of conventional materials, wear properties of material follow Archard's law which is defined as the following:

$$dV = \frac{KP}{H}dx\tag{11}$$

Where dV is the wear loss of material, P is load, H is hardness, K is wear resistance factor and dx is the wear distance (scratch length).

According to the relation mentioned above, materials with high hardness show lower wear volume or higher wear resistance. In the present work, BMG320 is found to have maximum hardness i.e., 8.3 GPa, followed by BMG350, BMG370 and as-cast metallic glass. Wear resistance of BMG320 is maximum in both the constant and progressive loading due to high hardness. However, for other metallic glasses, this trend is different. In case of constant loading, wear properties follow Archard's law with wear loss following the same trend as hardness and effective modulus. However, for progressive loading, this trend is quite

different with BMG320 having minimum wear loss, followed by as-cast BMG, BMG350 and BMG370. Therefore, it can be concluded that metallic glasses do not follow the Archard's law or in other words wear behavior of the metallic glasses is dependent not only on the hardness but on the combination of hardness and fracture toughness both as well as loading conditions. Based on this observation, the next section calculates the hardness and fracture toughness of the metallic glass samples by using scratch data in both constant and progressive loading.

3.6. Estimation of hardness and fracture toughness during constant and progressive loading scratch tests

To establish a relationship between wear and mechanical properties, the scratch hardness H_s (Eq. (6)) and the scratch fracture toughness K_s (Eq. (10)) of the BMG samples is calculated from the scratch data and are displayed in Fig. 9 for both constant and progressive loading conditions.

It is evident from Fig. 9 that the hardness determined from indentation, scratching with constant and progressive loading follows the same trend, revealing a correlation between the mechanical and the wear behavior of the metallic glasses. Since H_s is a direct measure of the wear resistance of a material, the lower scratch width and higher scratch hardness for BMG320 (shown in Figs. 3 and 9) for both constant and progressive loading makes it the most wear resistant metallic glass with a lower wear volume and wear rate than the other samples (Figs. 3 and 7). With an increase in the fictive temperature, scratch widths increase due to reduced structural relaxation and entrapment of free volume, and thus H_s decreases. During constant loading, K_s is highest for BMG320 (i. e., 48.9 MPam^{0.5}) followed by as-cast BMG (42.5 MPam^{0.5}), BMG350 (40.1 MPam^{0.5}), and BMG370 (39.8 MPam^{0.5}). In the case of progressive loading, K_s is also highest for BMG320 (i.e., 52.2 MPam^{0.5}) followed by as-cast (32.2 MPam^{0.5}), BMG350 (26.7 MPam^{0.5}), and BMG370 (17.8

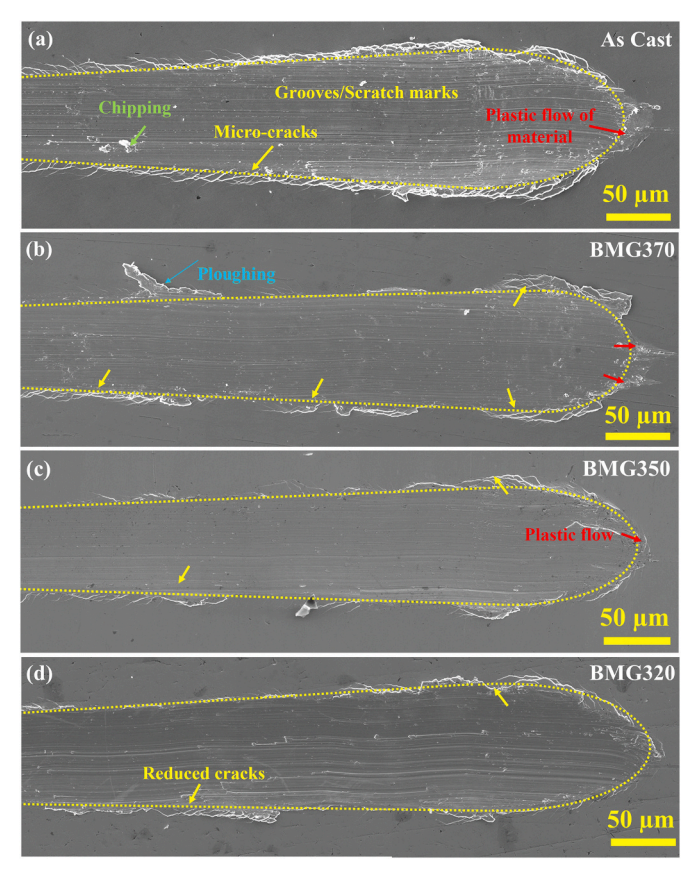


Fig. 8. Representative SEM micrographs of the scratches on BMGs with different fictive temperatures during scratch testing at progressive loading condition.

MPam^{0.5}) because of the change in fracture mode and enhanced content of free volume entrapment in the structure, which changes the energy dissipation mechanisms and thus the fracture toughness. $K_{\rm C}$ calculated from the scratch data also follows the fracture toughness calculated from the SENB method, as reported in the previous literature [34]. It is worth mentioning here that the scratch hardness and scratch fracture toughness values are higher than the microhardness and single edge notch beam fracture toughness values calculated in a previous study [34] because indentation methods generally overestimate these values.

4. Conclusions

In this study, samples made from $\rm Zr_{44}Ti_{11}Cu_{10}Ni_{10}Be_{25}$ bulk metallic glass with different fictive temperatures $\it T_f$ ($\it T_f = 320$ °C, 350 °C and 370 °C) have been analyzed for their mechanical and wear properties. The

important conclusions drawn from the results of the present study are listed below:

- XRD analysis confirmed their amorphous structure except for one sample (labeled as 370FC, Fig. A1) which was intentionally crystallized.
- 2. Plastic energy to total energy ratios calculated from the area under load-displacement curves reveals that the BMG320 has lowest plasticity (energy ratio = 0.59), leading to the highest hardness (8.3 GPa) and effective elastic modulus (144 GPa) among all samples investigated. Increased resistance to atomic flow due to enhanced structural relaxation leads to the improved mechanical behavior of BMG320.
- 3. Lower plasticity, higher hardness, and elastic modulus of BMG320 make it to be the most wear-resistant in both constant and progressive loading conditions, featuring the highest scratch hardness and lowest wear volume and wear rate of all samples investigated. Its enhanced hardness and most compact structural arrangement among the glassy samples result in a reduced crack formation and plastic deformation that increases its wear resistance compared to the other metallic glasses tested.
- 4. As $T_{\rm f}$ increases from 320 °C (0.91 $T_{\rm g}$) to 350 °C (0.99 $T_{\rm g}$) and ultimately 370 °C (1.05 $T_{\rm g}$), the higher degree of free volume entrapped in the material causes the plasticity of the samples to increase, which leads to a decreased wear resistance. Linear grooves at the center of the scratch and shear bands at the edge of the scratch traces confirm the wear mechanism to be abrasive wear.
- 5. Bulk metallic glasses in the present study do not follow Archard's wear law, however, a good combination of hardness and fracture toughness is required to predict the wear behavior.

Therefore, under corrosive wear environments, BMG320 with a higher degree of structural relaxation, high hardness and elastic modulus, and highest wear resistance can be utilized for better performance than other metallic glasses discussed in the present study.

Author contribution

A.D and K.B conceived and directed the work and obtained the funding together with U.D.S. A. D prepared the samples. S.B. and A.N. performed all the experiments and analyzed the data with help from R.S. S.B, A.N, A.D., K.B., and U.D.S. collaborated to compose the manuscript. All authors discussed and commented on the manuscript.

Declaration of competing interest

The authors declare that they have no known competing financial interests or personal relationships that could have appeared to influence the work reported in this paper.

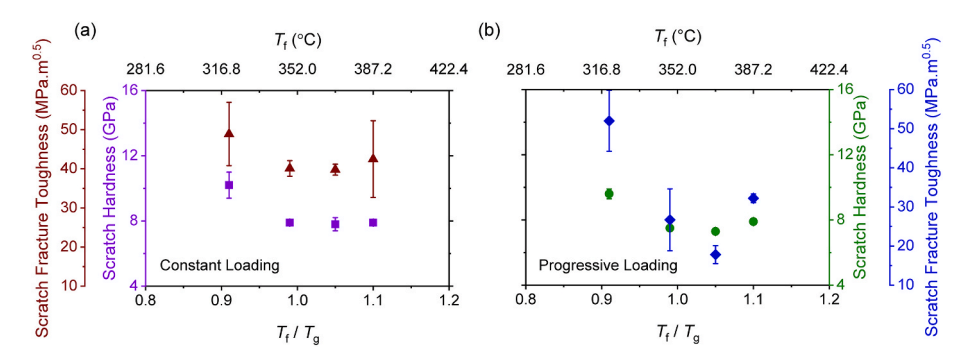


Fig. 9. Graphs illustrating the scratch hardness H_S and fracture toughness K_S obtained from scratch tests as a function of T_f for (a) Constant loading and (b) Progressive loading.

Acknowledgements

The authors would like to acknowledge the Advance Center for Materials Science (ACMS), IIT Kanpur, for providing micro-scratch, SEM, and other facilities to conduct this study. Work carried out at Yale University was supported by the National Science Foundation of the United States (Grant No. NSF CMMI-1901959).

APPENDIX

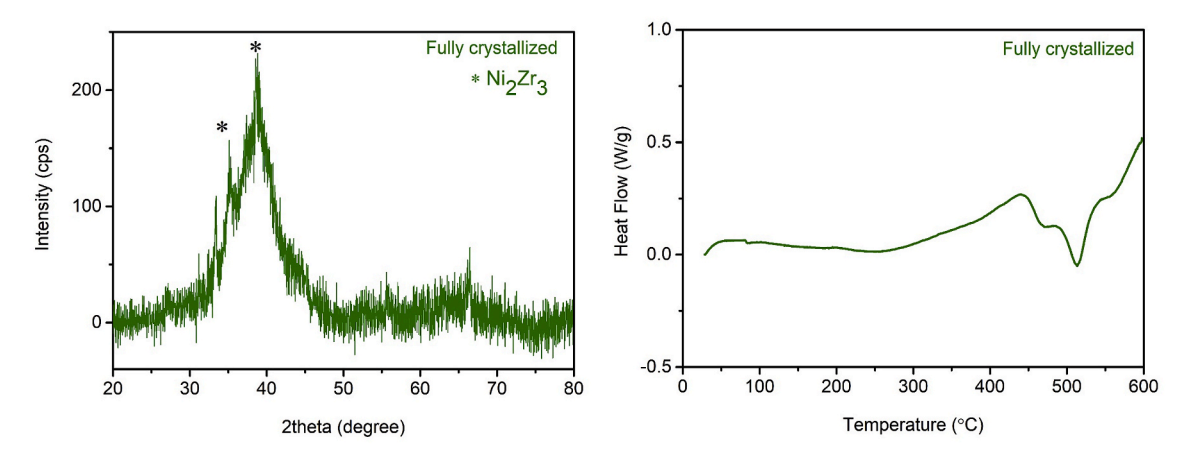


Fig. A1. Structural and thermal state of 370FC revealed by (a) XRD pattern and (b) DSC plot.

Table A1Mechanical properties of fully crystallized sample

Sample ID	Hardness (GPa)	Elastic Modulus (GPa)	PE/TE
370FC	8.4 ± 0.1	98.6 ± 1.2	0.64

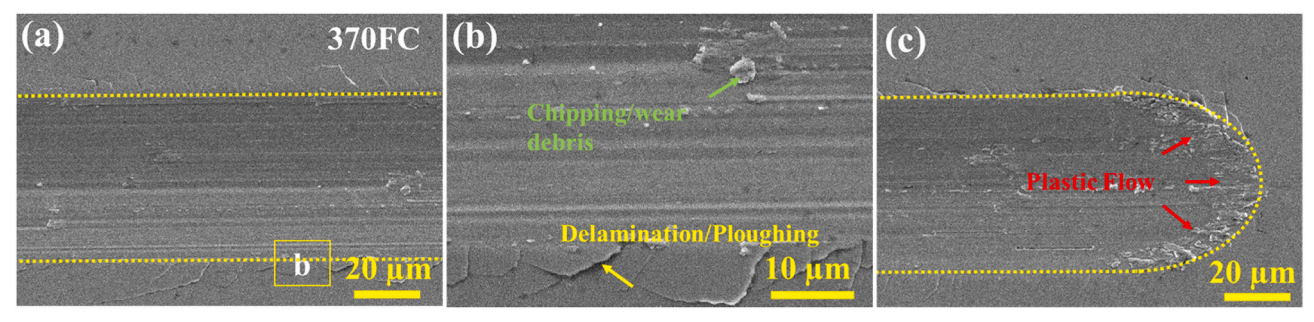


Fig. A2. SEM micrographs of the worn surface of 370FC revealing the presence of chipping, ploughing, and plastic flow of material confirming the wear mechanism to be abrasive wear with plastic deformation.

Table A2Wear properties of fully crystallized sample

Scratch Condition	CoF	Scratch width, w (µm)	Penetration depth, d (μm)	Scratch Hardness, H _s (GPa)	$Wv_{exp.}$ $(10^{-5}$ mm ³)	$Wr_{exp.}$ (10^{-3} mm ³ /Nm)	Scratch Fracture toughness (MPa.m ^{0.5})
Constant Load 10 N	0.25	51.7 ± 0.7	1.6 ± 0.1	9.5 ± 0.3	3.8 ± 0.2	3.8 ± 0.2	2.7 ± 0.1
Progressive Loading, 0.5–25 N	0.01-0.4	84.5 ± 0.8	17.5 ± 1.9	9.0 ± 0.2	5.0 ± 1.0	2.0 ± 0.4	6.1 ± 0.8

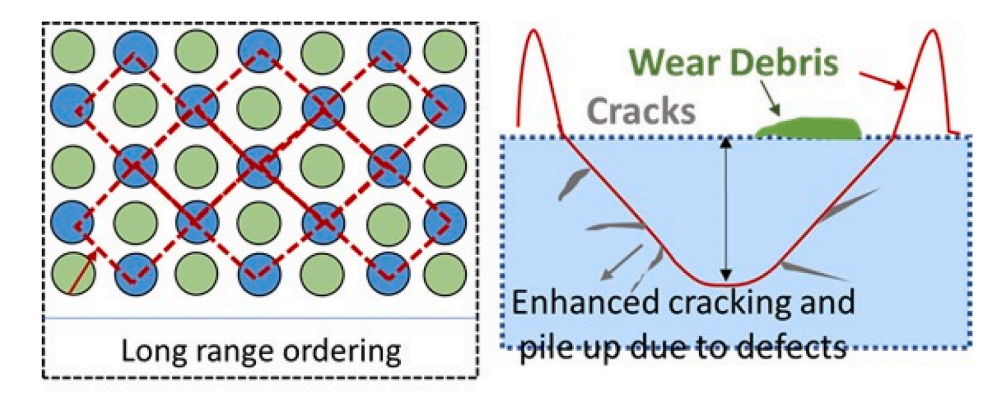


Fig. A3. Schematic representation of long-range ordering and wear mechanism in fully crystallized sample. Where blue and green spheres represent the atoms which are shown in different colors to represent the long and short-range ordering in the structure.

References

- W. Klement, R.H. Willens, P.O.L. Duwez, Non-crystalline structure in solidified gold-silicon alloys, Nature 187 (1960) 869–870.
- [2] A.I.C. Suryanarayana, Bulk Metallic Glasses, second ed., CRC Press, Taylor and Francis Group, 2010.
- [3] A.L. Greer, E. Ma, Bulk metallic glasses: at the cutting edge of metals research, MRS Bull. 32 (2011) 611–619.
- [4] J. Schroers, W.L. Johnson, Ductile bulk metallic glass, Phys. Rev. Lett. 93 (2004)
- [5] W.H. Wang, C. Dong, C.H. Shek, Bulk metallic glasses, Mater. Sci. Eng. R Rep. 44 (2004) 45–89.
- [6] H.S. Chen, Thermodynamic considerations on the formation and stability of metallic glasses, Acta Metall. 22 (1974) 1505–1511.
- [7] H.W. Kui, A.L. Greer, D. Turnbull, formation of bulk metallic-glass by fluxing, Appl. Phys. Lett. 45 (1984) 615–616.
- [8] M.C. Lee, W.L. Johnson, A two-dimensional phase separation on the spherical surface of the metallic glass Au₅₅Pb_{22.5}Sb_{22.5}, Appl. Phys. Lett. 41 (1982) 1054–1056.
- [9] P.L. Michael Miller, Bulk Metallic Glasses an Overview, Springer, 2008.
- [10] A. Datye, S.A. Kube, D. Verma, J. Schroers, U.D. Schwarz, Accelerated discovery and mechanical property characterization of bioresorbable amorphous alloys in the Mg-Zn-Ca and the Fe-Mg-Zn systems using high-throughput methods, J. Mater. Chem. B 7 (2019) 5392–5400.
- [11] A.L. Greer, K.L. Rutherford, I.M. Hutchings, Wear resistance of amorphous alloys and related materials, Int. Mater. Rev. 47 (2013) 87–112.
- [12] C.A. Angell, Formation of glasses from liquids and biopolymers, Science 267 (1995) 1924–1935.
- [13] Y.H. Liu, D. Wang, K. Nakajima, W. Zhang, A. Hirata, T. Nishi, A. Inoue, M. W. Chen, Characterization of nanoscale mechanical heterogeneity in a metallic glass by dynamic force microscopy, Phys. Rev. Lett. 106 (2011) 125504.
- [14] C.A. Schuh, T.C. Hufnagel, U. Ramamurty, Overview No.144 mechanical behavior of amorphous alloys, Acta Mater. 55 (2007) 4067–4109.
- [15] Y. Du, Q. Zhou, Q. Jia, Y.D. Shi, H.F. Wang, J. Wang, Imparities of shear avalanches dynamic evolution in a metallic glass, Mater Res Lett 8 (2020) 357–363.
- [16] P.J. Blau, Friction and wear of a Zr-based amorphous metal alloy under dry and lubricated conditions, Wear 250 (2001) 431–434.
- [17] M. Anis, W.M. Rainforth, H.A. Davies, Wear behaviour of rapidly solidified $Fe_6Cr_{18}Mo_2B_{12}$ alloys, Wear 172 (1994) 135–145.
- [18] R. Salehan, H.R. Shahverdi, R. Miresmaeili, Effects of annealing on the tribological behavior of Zr₆₀Cu₁₀Al₁₅Ni₁₅ bulk metallic glass, J. Non-Cryst. Solids 517 (2019) 127–136.
- [19] Y. Liu, Y.T. Zhu, X.K. Luo, Z.M. Liu, Wear behavior of a Zr-based bulk metallic glass and its composites, J. Alloys Compd. 503 (2010) 138–144.
- [20] J. Bhatt, S. Kumar, C. Dong, B.S. Murty, Tribological behaviour of $Cu_{60}Zr_{30}Ti_{10}$ bulk metallic glass, Mat Sci Eng a-Struct 458 (2007) 290–294.
- [21] Z. Parlar, M. Bakkal, A.J. Shih, Sliding tribological characteristics of Zr-based bulk metallic glass, Intermetallics 16 (2008) 34–41.
- [22] Q. Zhou, W. Han, D. Luo, Y. Du, J. Xie, X.-Z. Wang, Q. Zou, X. Zhao, H. Wang, B. D. Beake, Mechanical and Tribological Properties of Zr–Cu–Ni–Al Bulk Metallic Glasses with Dual-phase Structure, Wear, 2021, pp. 474–475.
- [23] G. Kumar, P. Neibecker, Y.H. Liu, J. Schroers, Critical fictive temperature for plasticity in metallic glasses, Nat. Commun. 4 (2013) 1536.
- [24] P.Y. Tian, N.W. Khun, S.B. Tor, E.J. Liu, Y. Tian, Tribological behavior of Zr-based bulk metallic glass sliding against polymer, ceramic, and metal materials, Intermetallics 61 (2015) 1–8.
- [25] A.Q. Tool, relation between inelastic deformability and thermal expansion of glass in its annealing range, J. Am. Ceram. Soc. 29 (1946) 240–253.
- [26] Y. Waseda, T. Egami, Effect of low-temperature annealing and deformation on the structure of metallic glasses by X-ray-diffraction, J. Mater. Sci. 14 (1979) 1249–1253.

- [27] F. Zhang, X.C. Wang, P. Deng, X.M. Qin, J. Tan, The evolution of structural and elastic properties of a Zr-based metallic glass upon annealing below glass transition temperature, Int. J. Mod. Phys. B 33 (2019).
- [28] B.B. Medeiros, M.M. Medeiros, J. Fornell, J. Sort, M.D. Baró, A.M. Jorge, Nanoindentation response of Cu–Ti based metallic glasses: comparison between ascast, relaxed and devitrified states, J. Non-Cryst. Solids 425 (2015) 103–109.
- [29] J.C. Qiao, J.M. Pelletier, C. Esnouf, Y. Liu, H. Kato, Impact of the structural state on the mechanical properties in a Zr–Co–Al bulk metallic glass, J. Alloys Compd. 607 (2014) 139–149.
- [30] M. Stoica, N. Van Steenberge, J. Bednarcik, N. Mattern, H. Franz, J. Eckert, Changes in short-range order of Zr₅₅Cu₃₀Al₁₀Ni₅ and Zr₅₅Cu₂₀Al₁₀Ni₁₀Ti₅ BMGs upon annealing, J. Alloys Compd. 506 (2010) 85–87.
- [31] W.J. Wright, T.C. Hufnagel, W.D. Nix, Free volume coalescence and void formation in shear bands in metallic glass, J. Appl. Phys. 93 (2003) 1432–1437.
- [32] W. Zhao, J.L. Cheng, H. cheng, G. Li, Effect of low-temperature annealing on the structure and mechanical properties of Zr–Cu metallic glasses, Mater. Sci. Eng., A 673 (2016) 239–242.
- [33] A. Datye, J. Ketkaew, J. Schroers, U.D. Schwarz, Effect of the fictive temperature on the modulus, hardness, yield strength, dynamic mechanical and creep response of Zr44Ti11Cu10Ni10Be25 metallic glasses, J. Alloys Compd. (2020) 819.
- [34] J. Ketkaew, W. Chen, H. Wang, A. Datye, M. Fan, G. Pereira, U.D. Schwarz, Z. Liu, R. Yamada, W. Dmowski, M.D. Shattuck, C.S. O'Hern, T. Egami, E. Bouchbinder, J. Schroers, Mechanical glass transition revealed by the fracture toughness of metallic glasses, Nat. Commun. 9 (2018) 3271.
- [35] H.T. Duan, Y. Wu, H. Meng, J.P. Wang, J.S. Tu, H.C. Kou, Y. Li, T.B. Zhang, J. Li, Tribological properties of Zr_{41.25}Ti_{13.75}Ni₁₀Cu_{12.5}Be_{22.5} bulk metallic glasses under different conditions, J. Alloys Compd. 528 (2012) 74–78.
- [36] H.T. Duan, J.S. Tu, S.M. Du, H.C. Kou, Y. Li, J.P. Wang, Z.W. Chen, J. Li, Tribological properties of Ti₄₀Zr₂₅Ni₈Cu₉Be₁₈ bulk metallic glasses under different conditions, Mater. Des. 32 (2011) 4573–4579.
- [37] B. Prakash, Abrasive wear behaviour of Fe, Co and Ni based metallic glasses, Wear 258 (2005) 217–224.
- [38] N.H. Tariq, B.A. Hasan, J.I. Akhter, F. Ali, Mechanical and tribological properties of Zr–Al–Ni–Cu bulk metallic glasses, J. Alloys Compd. 469 (2009) 179–185.
- [39] G. Kumar, J. Blawzdziewicz, J. Schroers, Controllable nanoimprinting of metallic glasses: effect of pressure and interfacial properties, Nanotechnology (2013) 24.
- [40] Z. Chen, A. Datye, G.H. Simon, C. Zhou, S.A. Kube, N.J. Liu, J.B. Liu, J. Schroers, U. D. Schwarz, Atomic-scale imprinting by sputter deposition of amorphous metallic films, Acs Appl Mater Inter 12 (2020) 52908–52914.
- [41] C. Zhou, A. Datye, Z. Chen, G.H. Simon, X.Z. Wang, J. Schroers, U.D. Schwarz, Atomic imprinting in the absence of an intrinsic length scale, Apl. Mater. 8 (2020).
- [42] P. Nagpal, N.C. Lindquist, S.H. Oh, D.J. Norris, Ultrasmooth patterned metals for plasmonics and metamaterials, Science 325 (2009) 594–597.
- [43] R.C. Sekol, G. Kumar, M. Carmo, F. Gittleson, N. Hardesty-Dyck, S. Mukherjee, J. Schroers, A.D. Taylor, Bulk metallic glass micro fuel cell, Small 9 (2013) 2081–2085.
- [44] L.M. Cox, A.M. Martinez, A.K. Blevins, N. Sowan, Y.F. Ding, C.N. Bowman, Nanoimprint lithography: emergent materials and methods of actuation, Nano Today 31 (2020).
- [45] A.J.E.C.T. Moynihan, M.A. Debolt, Dependence of the fictive temperature of glass on cooling rate, J. Am. Ceram. Soc. 59 (1976) 12–16.
- [46] G.S. Fulcher, Analysis of recent measurements of the viscosity of glasses. II, J. Am. Ceram. Soc. 8 (1925) 789–794.
- [47] T. Waniuk, J. Schroers, W.L. Johnson, Timescales of crystallization and viscous flow of the bulk glass-forming Zr-Ti-Ni-Cu-Be alloys, Phys. Rev. B 67 (2003).
- [48] M.E. Launey, R. Busch, J.J. Kruzic, Effects of free volume changes and residual stresses on the fatigue and fracture behavior of a Zr-Ti-Ni-Cu-Be bulk metallic glass, Acta Mater. 56 (2008) 500-510.
- [49] Y.L. Gao, J. Shen, J.F. Sun, G. Wang, D.W. Xing, H.Z. Xian, B.D. Zhou, Crystallization behavior of ZrAlNiCu bulk metallic glass with wide supercooled liquid region, Mater. Lett. 57 (2003) 1894–1898.

[50] S. Cardinal, J.M. Pelletier, M. Eisenbart, U.E. Klotz, Influence of crystallinity on thermo-process ability and mechanical properties in a Au-based bulk metallic glass, Mat Sci Eng a-Struct 660 (2016) 158–165.

- [51] J. Lendvai, J. Gubicza, J.L. Labar, Z. Kuli, Effect of crystallization on the deformation behavior of a Zr-based bulk metallic glass, Int. J. Mater. Res. 100 (2009) 439–442.
- [52] W.C. Oliver, G.M. Pharr, An improved technique for determining hardness and elastic-modulus using load and displacement sensing indentation experiments, J. Mater. Res. 7 (1992) 1564–1583.
- [53] A. Datye, L. Li, W. Zhang, Y.J. Wei, Y.F. Gao, G.M. Pharr, Extraction of anisotropic mechanical properties from nanoindentation of SiC-6H single crystals, J Appl Mech-T Asme 83 (2016).
- [54] S. Bajpai, R. Kundu, K. Balani, Effect of B4C reinforcement on microstructure, residual stress, toughening and scratch resistance of (Hf, Zr)B2 ceramics, Mater. Sci. Eng., A (2020) 796.
- [55] A.T. Akono, N.X. Randall, F.J. Ulm, Experimental determination of the fracture toughness via microscratch tests: application to polymers, ceramics, and metals, J. Mater. Res. 27 (2012) 485–493.
- [56] Z. Evenson, R. Busch, Equilibrium viscosity, enthalpy recovery and free volume relaxation in a Zr₄₄Ti₁₁Ni₁₀Cu₁₀Be₂₅ bulk metallic glass, Acta Mater. 59 (2011) 4404–4415.

- [57] A. Slipenyuk, J. Eckert, Correlation between enthalpy change and free volume reduction during structural relaxation of Zr₅₅Cu₃₀Al₁₀Ni₅ metallic glass, Scripta Mater. 50 (2004) 39–44.
- [58] O. Haruyama, Y. Nakayama, R. Wada, H. Tokunaga, J. Okada, T. Ishikawa, Y. Yokoyama, Volume and enthalpy relaxation in Zr₅₅Cu₃₀Ni₅Al₁₀ bulk metallic glass, Acta Mater. 58 (2010) 1829–1836.
- [59] A. Datye, H.T. Lin, Energy analysis of spherical and Berkovich indentation contact damage in commercial polycrystalline silicon carbide, Ceram. Int. 43 (2017) 800–809.
- [60] G. Stachowiak, Bikramjit basu and mitjan kalin: tribology of ceramics and composites: a materials science perspective, Tribol. Lett. 63 (2016).
- [61] Y. Wang, L.L. Shi, D.L. Duan, S. Li, J. Xu, Tribological properties of Zr₆₁Ti₂Cu₂₅Al₁₂ bulk metallic glass under simulated physiological conditions, Mater Sci Eng C Mater Biol Appl 37 (2014) 292–304.
- [62] K. Miyoshi, D.H. Buckley, Microstructure and surface-chemistry of amorphousalloys important to their friction and wear behavior, Wear 110 (1986) 295–313.
- [63] E. Fleury, S.M. Lee, H.S. Ahn, W.T. Kim, D.H. Kim, Tribological properties of bulk metallic glasses, Mat Sci Eng a-Struct 375 (2004) 276–279.